

Title	Origin of the strong interaction between polar molecules and copper(II) paddle-wheels in metal organic frameworks
Authors	Ongari, Daniele;Tiana, Davide;Stoneburner, Samuel J.;Gagliardi, Laura;Smit, Berend
Publication date	2017-06-27
Original Citation	Ongari, D., Tiana, D., Stoneburner, S. J., Gagliardi, L. and Smit, B. (2017) 'Origin of the Strong Interaction between Polar Molecules and Copper(II) Paddle-Wheels in Metal Organic Frameworks', The Journal of Physical Chemistry C, 121(28), pp. 15135-15144.
Type of publication	Article (peer-reviewed)
Link to publisher's version	http://dx.doi.org/10.1021/acs.jpcc.7b02302 - 10.1021/acs.jpcc.7b02302
Rights	© 2017 American Chemical Society. This is an open access article published under an ACS AuthorChoice License, which permits copying and redistribution of the article or any adaptations for non-commercial purposes - https://pubs.acs.org/page/policy/authorchoice_termsofuse.html
Download date	2025-04-10 04:27:48
Item downloaded from	https://hdl.handle.net/10468/6429



UCC

University College Cork, Ireland
 Coláiste na hOllscoile Corcaigh

The Origin of the Strong Interaction Between Polar Molecules and Copper (II) Paddle-Wheels in Metal Organic Frameworks

Daniele Ongari,^a Davide Tiana,^a Sam Stoneburner,^b Laura Gagliardi^{b*} and Berend Smit^{a*}

^a *Laboratory of Molecular Simulation, Institut des Sciences et Ingénierie Chimiques, Ecole Polytechnique Fédérale de Lausanne (EPFL), Rue de l'Industrie 17, CH-1951 Sion, Valais, Switzerland*

^b *Department of Chemistry, Chemical Theory Center, and Supercomputing Institute, University of Minnesota, Minneapolis, Minnesota 55455, United States*

Supporting Information

Table of Contents:

1. Results from multireference calculations
Discussion of active spaces
(10,10) active space orbitals (Figure S1)
Electronic configuration weight in (2,2)CASPT2 (Table S1)
Absolute CASSCF and CASPT2 energies (Table S2-S11)
2. DFT derived point charges
REPEAT charges (Table S12)
Bader charges (Table S13)
3. Fitting of the Cu-O interaction
Comparison MP2 and fitted interaction potential (Figure S2)
4. Classical simulations' details
5. Results from classical simulations in HKUST-1
CO₂ occupations (Figure S3)
High pressure isotherms (Figure S4)
Isotherms from 283K to 343K (Figure S5)
Heat of desorption (Figure S6)
6. Geometries of the M06-L/cc-pVDZ optimized structures
Cu₂(formate)₄ – CO₂ linear
Cu₂(formate)₄ – CO₂ tilted
Cu(formate)₂ – CO₂ linear
Cu(formate)₂ – CO₂ tilted

1. Results from multireference calculations

Several different active spaces were attempted, but only the (2,2) orbitals (Figure 7) were clearly necessary. In terms of energy, the next four highest occupied orbitals and their corresponding unoccupied orbitals were all π/π^* orbitals of the O and C atoms of the paddlewheels, resulting in the (10,10) active space shown in Figure S1. Including only some of them resulted in an arbitrarily imbalanced active space that did not realistically reflect the symmetry of the molecule or the near-degeneracy of the orbitals. Including additional orbitals beyond or instead of those of the (10,10) yielded no interesting results – the occupation numbers of the orbitals were very close to 2 or 0, and the binding energies were almost always quite close to those calculated with the (2,2) active space.

In order to maintain balance in calculating the interaction energies, the isolated CO_2 was calculated with a (0,0) active space, while the $\text{Cu}_2(\text{formate})_4$ and $\text{Cu}_2(\text{formate})_4\text{-CO}_2$ were calculated with either (2,2) or (10,10). CO_2 is a closed-shell singlet, so there is no expectation of any multireference character in the isolated CO_2 subsystem.

Figure S1. Orbitals of the (10,10) active space, BS2 basis set, with the $\text{Cu}_2(\text{formate})_4$. The (10,10) active space looked quite similar for other basis sets and for the $\text{Cu}_2(\text{formate})_4\text{-CO}_2$ supersystems. Occupation numbers are below each orbital.

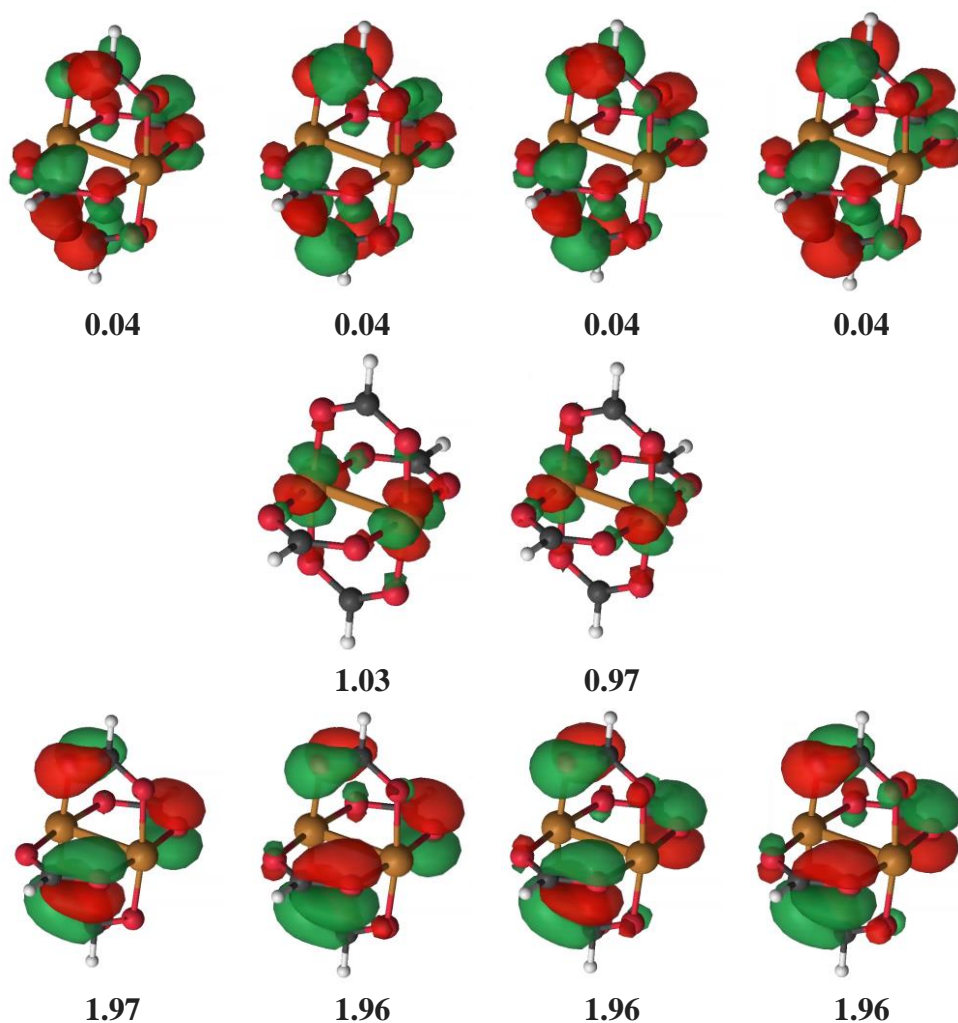


Table S1. Wave function description in the case of the (2,2) active space for both the titled and linear systems at equilibrium. Dominant electronic configurations with their weight in the total wave function.

Electronic configuration	% Weight
MO1 ² MO2 ⁰	0.51
MO1 ⁰ MO2 ²	0.49

Table S2. Absolute CASSCF and CASPT2 energies (Hartree) of the isolated CO₂, linear geometry, used to determine the binding energies reported in Table 4.

Basis set	Active space	CASSCF	CASPT2
BS1	(0,0)	-187.822846	-188.313273
BS2	(0,0)	-187.837740	-188.440743
BS3	(0,0)	-187.839851	-188.484601

Table S3. Absolute CASSCF and CASPT2 energies (Hartree) of the isolated CO₂, tilted geometry, used to determine the binding energies reported in Table 4.

Basis set	Active space	CASSCF	CASPT2
BS1	(0,0)	-187.822569	-188.313188
BS2	(0,0)	-187.837455	-188.440624
BS3	(0,0)	-187.839566	-188.484478

Table S4. Absolute CASSCF and CASPT2 energies (Hartree) of the isolated Cu₂(formate)₄ used to determine the binding energies reported in Table 4.

Basis set	Active space	CASSCF	CASPT2
BS1	(2,2)	-4059.968773	-4063.227939
BS1	(10,10)	-4060.049277	-4063.212558
BS2	(2,2)	-4060.055097	-4064.087188
BS2	(10,10)	-4060.136090	-4064.072438
BS3	(2,2)	-4060.060482	-4064.247098
BS3	(10,10)	-4060.141483	-4064.232340

Table S5. Absolute CASSCF and CASPT2 energies (Hartree) of the Cu₂(formate)₄-CO₂, linear geometry, used to determine the binding energies reported in Table 4.

Basis set	Active space	CASSCF	CASPT2
BS1	(2,2)	-4247.797689	-4251.557651
BS1	(10,10)	-4247.876957	-4251.543564
BS2	(2,2)	-4247.897307	-4252.540696
BS2	(10,10)	-4247.977185	-4252.527181
BS3	(2,2)	-4247.904638	-4252.743773
BS3	(10,10)	-4247.984527	-4252.730259

Table S6. Absolute CASSCF and CASPT2 energies (Hartree) of the $\text{Cu}_2(\text{formate})_4\text{-CO}_2$, tilted geometry, used to determine the binding energies reported in Table 4.

Basis set	Active space	CASSCF	CASPT2
BS1	(2,2)	-4247.798861	-4251.559923
BS1	(10,10)	-4247.878590	-4251.545223
BS2	(2,2)	-4247.898236	-4252.543039
BS2	(10,10)	-4247.978529	-4252.528944
BS3	(2,2)	-4247.905606	-4252.746666
BS3	(10,10)	-4247.985917	-4252.732487

Table S7. Absolute CASSCF and CASPT2 energies (Hartree) of the isolated CO_2 , linear geometry, in the basis set of the full $\text{Cu}_2(\text{formate})_4\text{-CO}_2$ linear geometry supersystem, used to determine the counterpoise corrections reported in Table 4.

Basis set	Active space	CASSCF	CASPT2
BS1	(0,0)	-187.823414	-188.318897
BS2	(0,0)	-187.837960	-188.442773
BS3	(0,0)	-187.839900	-188.485419

Table S8. Absolute CASSCF and CASPT2 energies (Hartree) of the isolated CO_2 , tilted geometry, in the basis set of the full $\text{Cu}_2(\text{formate})_4\text{-CO}_2$ tilted geometry supersystem, used to determine the counterpoise corrections reported in Table 4.

Basis set	Active space	CASSCF	CASPT2
BS1	(0,0)	-187.823253	-188.318981
BS2	(0,0)	-187.837678	-188.442790
BS3	(0,0)	-187.839609	-188.485428

Table S9. Absolute CASSCF and CASPT2 energies (Hartree) of the $\text{Cu}_2(\text{formate})_4\text{-CO}_2$, in the basis set of the full $\text{Cu}_2(\text{formate})_4\text{-CO}_2$ linear geometry supersystem, used to determine the counterpoise corrections reported in Table 4.

Basis set	Active space	CASSCF	CASPT2
BS1	(2,2)	-4059.970480	-4063.233025
BS1	(10,10)	-4060.050061	-4063.219018
BS2	(2,2)	-4060.055578	-4064.090787
BS2	(10,10)	-4060.135696	-4064.077335
BS3	(2,2)	-4060.060891	-4064.250660
BS3	(10,10)	-4060.141011	-4064.237202

Table S10. Absolute CASSCF and CASPT2 energies (Hartree) of the $\text{Cu}_2(\text{formate})_4\text{-CO}_2$, in the basis set of the full $\text{Cu}_2(\text{formate})_4\text{-CO}_2$ tilted geometry supersystem, used to determine the counterpoise corrections reported in Table 4.

Basis set	Active space	CASSCF	CASPT2
BS1	(2,2)	-4059.970579	-4063.234198
BS1	(10,10)	-4060.050182	-4063.220224
BS2	(2,2)	-4060.055607	-4064.091308
BS2	(10,10)	-4060.135737	-4064.077856
BS3	(2,2)	-4060.060906	-4064.251429
BS3	(10,10)	-4060.141044	-4064.237960

Table S11. Absolute CASSCF and CASPT2 triplet energies (Hartree) and singlet-triplet gaps (ΔE_{ST} , kJ/mol) of the $\text{Cu}_2(\text{formate})_4$, linear $\text{Cu}_2(\text{formate})_4\text{-CO}_2$, and tilted $\text{Cu}_2(\text{formate})_4\text{-CO}_2$ systems.

System	Basis set	Active space	CASSCF	CASPT2	CASPT2 ΔE_{ST}
$\text{Cu}_2(\text{formate})_4$	BS1	(2,2)	-4059.968773	-4063.227939	-3.0
$\text{Cu}_2(\text{formate})_4$	BS1	(10,10)	-4060.049277	-4063.212558	-2.9
$\text{Cu}_2(\text{formate})_4\text{-CO}_2$, linear	BS1	(2,2)	-4247.797689	-4251.557651	-3.4
$\text{Cu}_2(\text{formate})_4\text{-CO}_2$, linear	BS1	(10,10)	-4247.876957	-4251.543564	-3.5
$\text{Cu}_2(\text{formate})_4\text{-CO}_2$, tilted	BS1	(2,2)	-4247.798861	-4251.559923	-3.3
$\text{Cu}_2(\text{formate})_4\text{-CO}_2$, tilted	BS1	(10,10)	-4247.878590	-4251.545223	-3.6
$\text{Cu}_2(\text{formate})_4$	BS2	(2,2)	-4060.054968	-4064.086116	-2.8
$\text{Cu}_2(\text{formate})_4\text{-CO}_2$, linear	BS2	(2,2)	-4247.897182	-4252.539441	-3.3
$\text{Cu}_2(\text{formate})_4\text{-CO}_2$, tilted	BS2	(2,2)	-4247.898111	-4252.541817	-3.2

2. DFT derived point charges

Table S12. Comparison of point charges computed from PBEsol DFT calculation using the REPEAT scheme [1], and employed for the classical simulations.

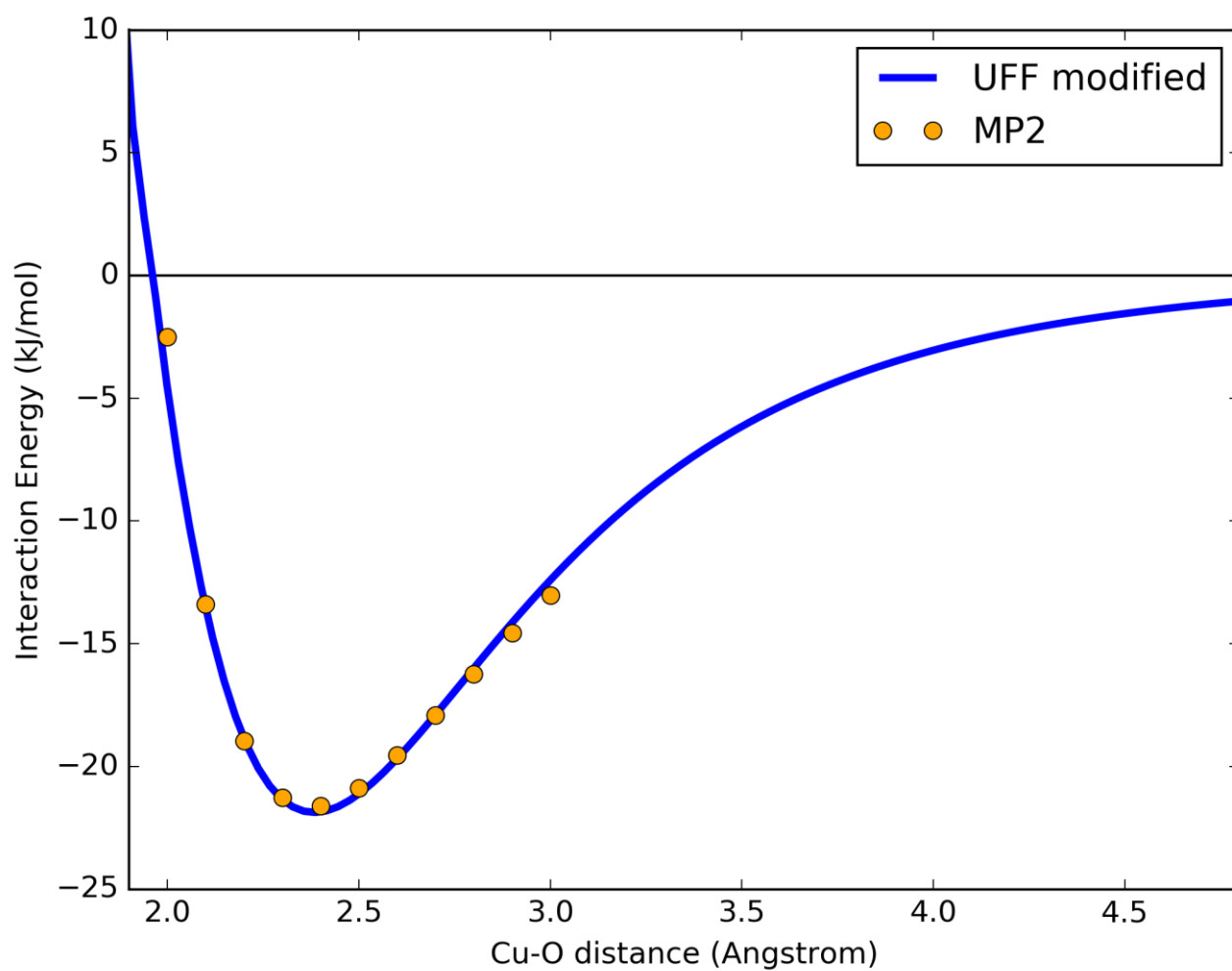
Atom type	HKUST-1	Cu ₂ formate ₄	Cu ₁ formate ₄
Cu	0.914	1.063	0.809
O (carboxylic)	-0.534	-0.618	-0.485
H (benzene)	0.159		
H (formate)		0.035	0.086
C (carboxylic)	0.586	0.668	0.480
C (benzene, CH)	0.062		
C (benzene, CC)	-0.196		

Table S13. Comparison of point charges computed from PBEsol DFT calculation using the Bader scheme [2]. The values computed were not used for simulation but only for compare the charges in the different structures, using a more chemically rigorous method. On the other hand, REPEAT point charges are fitted to reproduce the electric field created by the electron density and are more reliable for simulations.

Atom type	HKUST-1	Cu ₂ formate ₄	Cu ₁ formate ₄
Cu	1.035	1.088	1.035
O (carboxylic)	-1.068	-1.031	-1.018
H (benzene)	0.185		
H (formate)		0.037	0.085
C (carboxylic)	1.512	1.492	1.435
C (benzene, CH)	-0.011		
C (benzene, CC)	-0.066		

3. Fitting of the Cu-O interaction

Figure S2: Modified Cu-O interaction fitted on the MP2 linear scan for CO₂ and Cu₂(formate)₄



4. Classical simulations' details

For all the classical single point calculations and GCMC simulations, RASPA package [3] was used. Truncated potential with a cutoff of 13 Angstroms was employed, without tail corrections. Ewald method was used to model charges in periodic cells. For single point calculation on $\text{Cu}_2\text{formate}_4$ and $\text{Cu}_1\text{formate}_2$ we assumed a cubic unit cell of 100 angstrom length to remove the effect of periodic boundaries and Coulombic interactions were modelled with truncating the potential at 30 Angstroms instead of using the Ewald method. For the Gran Canonical Monte Carlo simulations, 50.000 cycles were used to equilibrate the system and other 50.000 cycles to collect statistics.

UFF [4] and DREIDING [5] parameters (12-6 Lennard-Jones potential) are listed in the following table:

Atom Type	UFF		DREIDING	
	Epsilon (K)	Sigma (angstrom)	Epsilon (K)	Sigma (angstrom)
H	22.14	2.57	7.65	2.85
C	52.84	3.43	47.86	3.47
O	30.20	3.12	48.16	3.03
Cu	2.52	3.11	Not included	Not included

TraPPE [6] parameters (12-6 Lennard Jones potential) and charges are listed in the following table:

Atom Type	Epsilon (K)	Sigma (angstrom)	Charge (au)
C	27.00	2.80	0.70
O	79.00	3.05	-0.35

To fit the Cu-O interaction, the “generic” potential was used in RASPA, instead of the 12-6 Lennard Jones potential. This potential is described by equation 3.94 from RASPA's user manual:

$$U = p_0 e^{-p_1 r} - \frac{p_2}{r^4} - \frac{p_3}{r^6} - \frac{p_4}{r^8} - \frac{p_5}{r^{10}} \quad (3.94)$$

6 arguments: p_0/k_B in units of K, p_1 in units of \AA^{-1} , p_2/k_B in units of K \AA^4 , p_3/k_B in units of K \AA^6 , p_4/k_B in units of K \AA^8 , and p_5/k_B in units of K \AA^{10} .

$$p_0 = 1\text{E}+8$$

$$p_1 = 4.19$$

$$p_2 = 0$$

$$p_3 = 3.196\text{E}+4 = 4 \cdot \text{Epsilon}_{\text{Cu-O}} \cdot (\text{Sigma}_{\text{Cu-O}})^6$$

(Lennard-Jones mixed parameters for Cu-O interaction in UFF)

$$p_4 = 5.0\text{E}+6$$

$$p_5 = 0$$

The potential for Cu-O distances inferior to 1.8 angstrom were fixed to $1\text{E}+15$ K to avoid the collapse of the potential to zero at a distance equal to zero between the two atoms.

5. Results from classical simulations in HKUST-1

Figure S3. CO₂ occupation at 1bar, 295K using the modified potential. Occupation of oxygen is shown in red with an isovalue for the surface equal to 0.25. Open metal, small pore window and small pore cage sites are occupied.

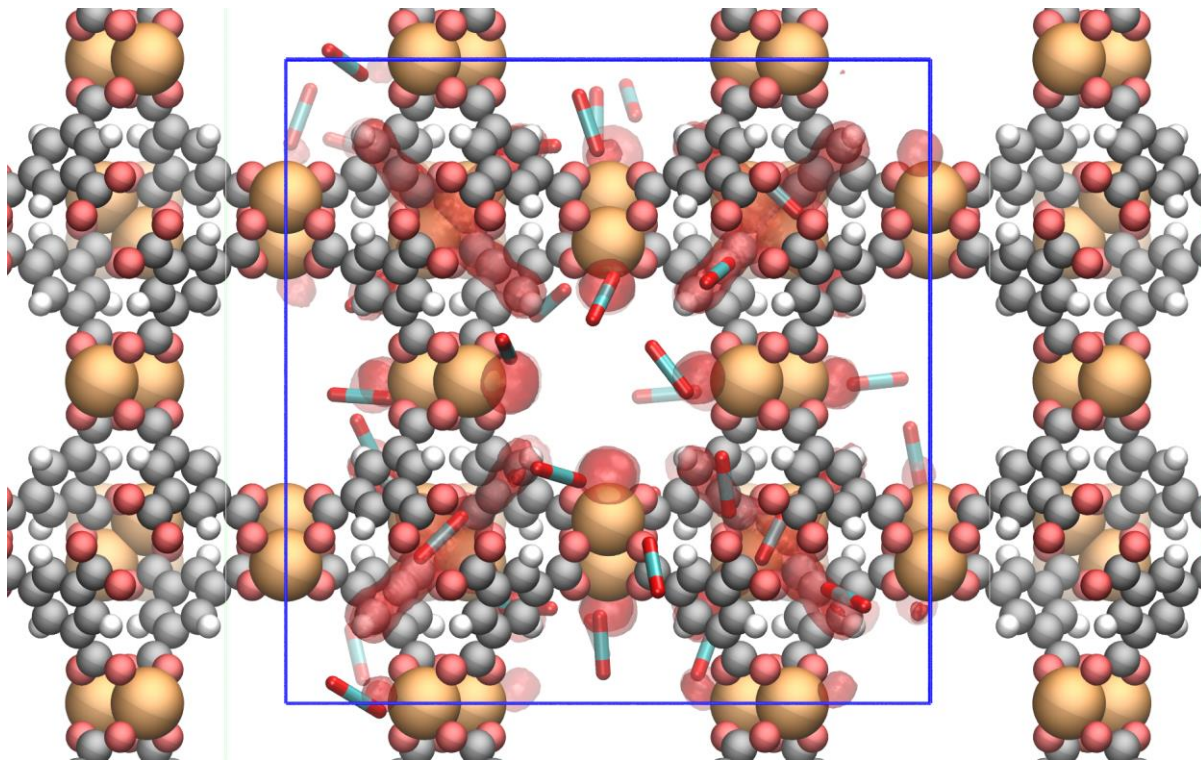


Figure S4. Comparison of simulated and experimental [7] 303K isotherms for a higher range of pressure. For pressures higher than 2 bar (which correspond to an uptake of ~ 2 carbon dioxide molecules per copper metal) our modified force field starts to overestimate the experimental isotherm. This can mean that the Cu-O potential derived from ROS-MP2 calculations in di-copper formate is predicting the proper interaction close to the optimal distance; however, the tail of the Cu-O potential is slightly overestimated at high distances, leading to a higher interaction at the center of the large and medium pores. On the experimental point of view, it is common for simulation to overestimate the saturation loading because we are not taking into account the defects of the crystal. In this case, Grajciar et al. reported a surface area of 1628 m²/g while the crystal we used for the simulation has a surface area of 1911 m²/g. We want to stress the fact that our correction to the Cu-O interaction is intended to improve the modelling of the low-pressure regime.

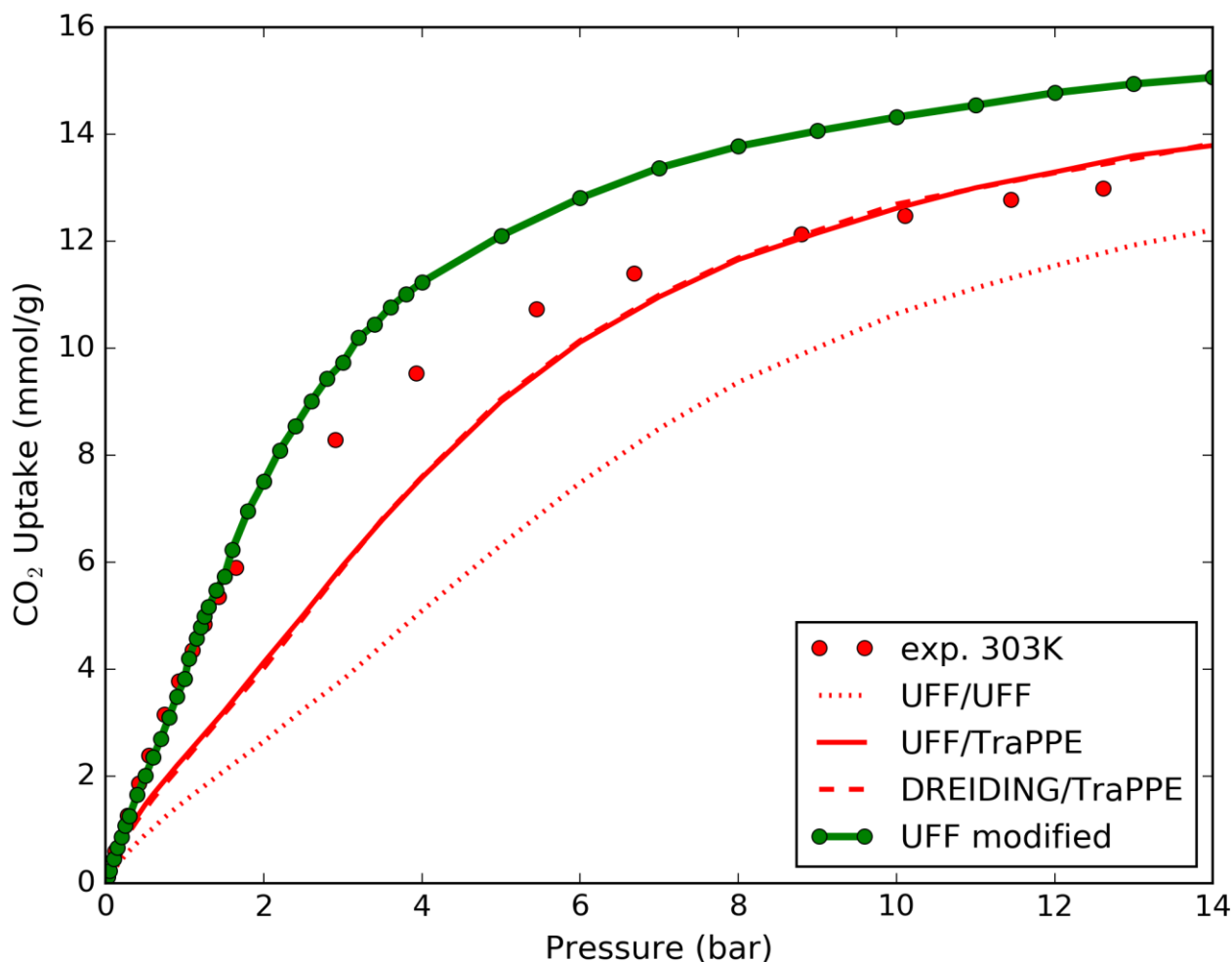


Figure S5. Comparison of simulated (modified UFF developed in this work, lines) and experimental (Aprea et al. [8], black markers) isotherms at different temperatures: 283, 293, 318 and 343 K. Our force field appears to be in good agreement with experiments over a range of temperature of 60K.

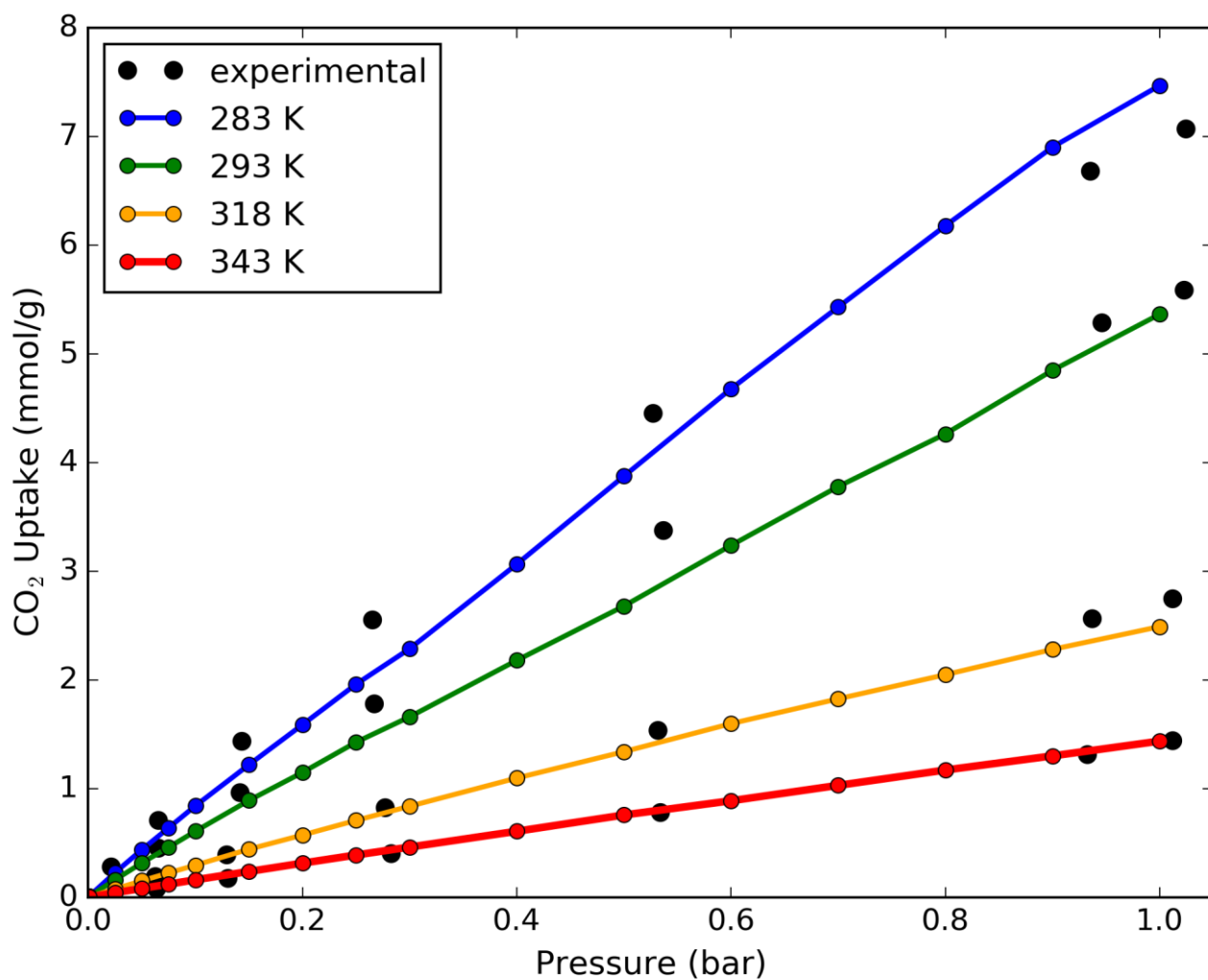
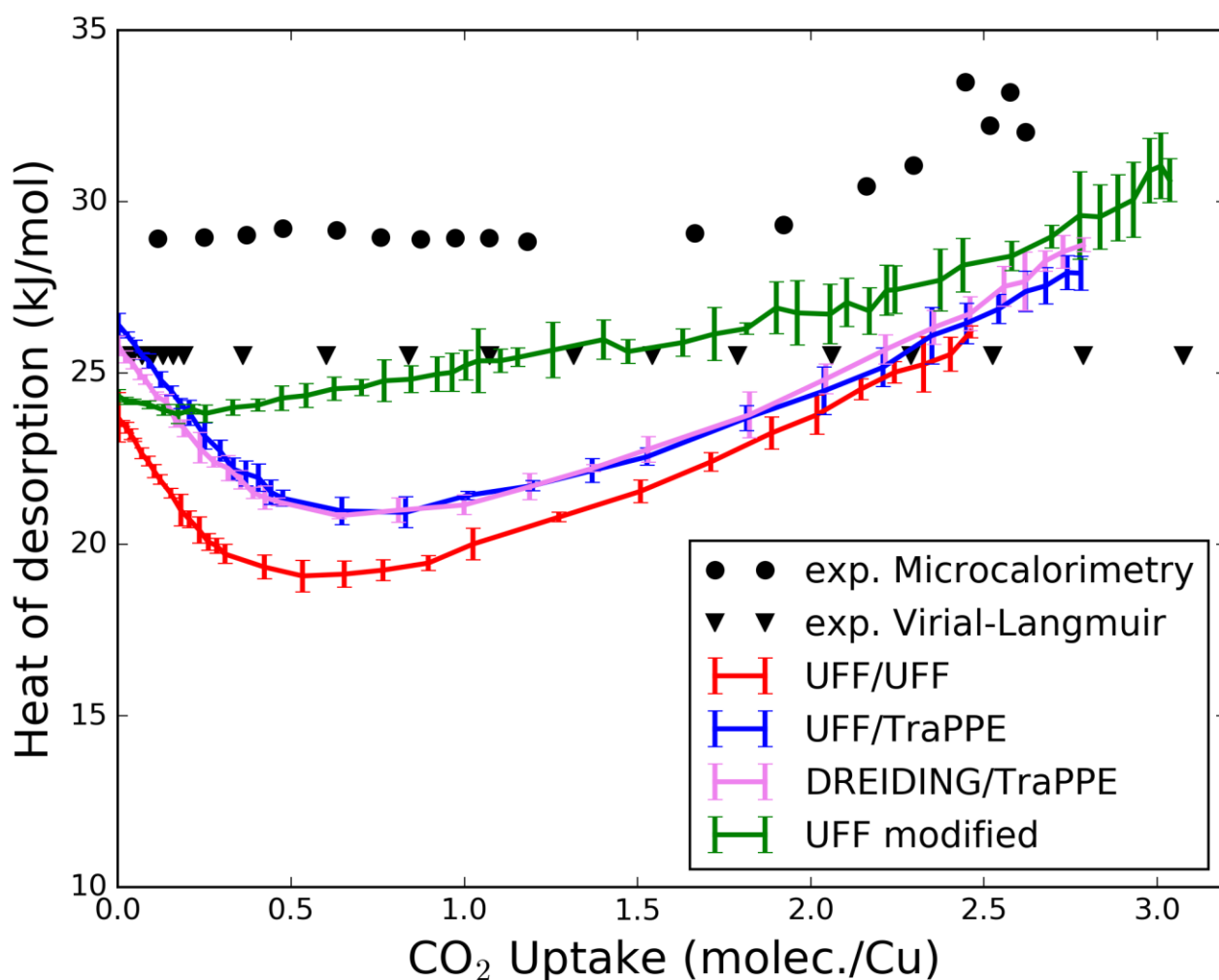


Figure S6. Heat of desorption of carbon dioxide in HKUST-1 computed experimentally with microcalorimetry at 303K (Grajciar et al. [7]) and with a Virial-Langmuir fitting from 295K, 318K and 353K isotherms (measurement from Chowdhury et al. [9], the heat of desorption has been computed by Krishna [10] after the conversion from excess to absolute uptake). The experimental measurement are compared to simulated values using different sets of parameters (computed from a GCMC run, considering the fluctuation of the energy with the number of particles along the simulation). The uptake is reported in molecules of CO₂ per copper atom, with 1 corresponding to 4.96 mmol/g. The UFF modified force field is more accurate than the standard ones to predict the experimental trend for the heat of desorption, despite the remarkable difference between the absolute values of the two measurements.



6. Geometries of the M06-L/cc-pVDZ optimized structures

Cu₂(formate)₄ - CO₂ linear

Cu	0.000000	0.000000	1.279062
Cu	0.000000	0.000000	-1.279062
C	0.000000	2.546196	0.000000
C	0.000000	-2.546196	0.000000
C	2.546196	0.000000	0.000000
C	-2.546196	0.000000	0.000000
H	0.000000	3.639038	0.000000
H	3.639038	0.000000	0.000000
H	0.000000	-3.639038	0.000000
H	-3.639038	0.000000	0.000000
O	0.000000	1.965949	1.152213
O	-1.965949	0.000000	1.152213
O	0.000000	-1.965949	1.152213
O	1.965949	0.000000	1.152213
O	0.000000	1.965949	-1.152213
O	1.965949	0.000000	-1.152213
O	0.000000	-1.965949	-1.152213
O	-1.965949	0.000000	-1.152213
O	0.000000	0.000000	3.679062
C	0.000000	0.000000	4.849062
O	0.000000	0.000000	6.019062

Cu₂(formate)₄ - CO₂ tilted

Cu	0.000000	0.000000	1.279062
Cu	0.000000	0.000000	-1.279062
C	0.000000	2.546196	0.000000
C	0.000000	-2.546196	0.000000
C	2.546196	0.000000	0.000000
C	-2.546196	0.000000	0.000000
H	0.000000	3.639038	0.000000
H	3.639038	0.000000	0.000000
H	0.000000	-3.639038	0.000000
H	-3.639038	0.000000	0.000000
O	0.000000	1.965949	1.152213
O	-1.965949	0.000000	1.152213
O	0.000000	-1.965949	1.152213
O	1.965949	0.000000	1.152213
O	0.000000	1.965949	-1.152213
O	1.965949	0.000000	-1.152213
O	0.000000	-1.965949	-1.152213
O	-1.965949	0.000000	-1.152213
O	0.388568	0.382205	3.631061
C	1.237370	1.155413	3.878149
O	2.067704	1.928184	4.150895

Cu(formate)₂ - CO₂ linear

Cu	0.000000	0.000000	0.000000
C	0.000000	2.323540	0.000000
C	0.000000	-2.323540	0.000000
H	0.000000	-3.427613	0.000000
H	0.000000	3.427613	0.000000
O	-1.095368	1.686653	0.000000
O	1.095368	1.686653	0.000000
O	1.095368	-1.686653	0.000000
O	-1.095368	-1.686653	0.000000
O	0.000000	0.000000	2.600000
C	0.000000	0.000000	3.770000
O	0.000000	0.000000	4.940000

Cu(formate)₂ - CO₂ tilted

Cu	0.000000	0.000000	0.000000
C	0.000000	2.323540	0.000000
C	0.000000	-2.323540	0.000000
H	0.000000	-3.427613	0.000000
H	0.000000	3.427613	0.000000
O	-1.095368	1.686653	0.000000
O	1.095368	1.686653	0.000000
O	1.095368	-1.686653	0.000000
O	-1.095368	-1.686653	0.000000
O	3.278298	0.009327	2.401491
C	2.112722	0.008841	2.450267
O	0.938756	0.008091	2.514749

References:

- 1) Campaná, C.; Mussard, B.; Woo, T. K. Electrostatic potential derived atomic charges for periodic systems using a modified error functional. *J. Chem. Theory Comput.* **2009**, 5, 2866–2878.
- 2) Otero-de-la Roza, A.; Johnson, E. R.; Luaña, V. Critic2: A program for real-space analysis of quantum chemical interactions in solids. *Comp. Phys. Comm.* **2014**, 185, 1007–1018.
- 3) Dubbeldam, D.; Calero, S.; Ellis, D. E.; Snurr, R. Q. RASPA: Molecular simulation software for adsorption and diffusion in flexible nanoporous materials. *Mol. Simul.* **2016**, 42, 81–101.
- 4) Rappé, A. K.; Casewit, C. J.; Colwell, K.; Goddard Iii, W.; Skiff, W. UFF, a full periodic table force field for molecular mechanics and molecular dynamics simulations. *J. Am. Chem. Soc.* **1992**, 114, 10024–10035.
- 5) Mayo, S. L.; Olafson, B. D.; Goddard, W. A. DREIDING: a generic force field for molecular simulations *J. of Phys. Chem.* **1990**, 94, 8897–8909.
- 6) Potoff, J. J.; Siepmann, J. I. Vapor–liquid equilibria of mixtures containing alkanes, carbon dioxide, and nitrogen. *AIChE J.* **2001**, 47, 1676–1682.
- 7) Grajciar, L.; Wiersum, A. D.; Llewellyn, P. L.; Chang, J.-S.; Nachtigall, P. Understanding CO₂ adsorption in CuBTC MOF: comparing combined DFT–ab initio calculations with microcalorimetry experiments. *J. Phys. Chem. C* **2011**, 115, 17925–17933.
- 8) Aprea, P.; Caputo, D.; Gargiulo, N.; Iucolano, F.; Pepe, F. Modeling carbon dioxide adsorption on microporous substrates: comparison between Cu-BTC metal-organic framework and 13X zeolitic molecular sieve. *J. Chem. Eng. Data* **2010**, 55, 3655–3661.
- 9) Chowdhury, P.; Mekala, S.; Dreisbach, F.; Gumma, S. Adsorption of CO, CO₂ and CH₄ on Cu-BTC and MIL-101 metal organic frameworks: Effect of open metal sites and adsorbate polarity. *Microporous Mesoporous Mater.* **2012**, 152, 246–252.
- 10) Krishna, R. Adsorptive separation of CO₂/CH₄/CO gas mixtures at high pressures. *Microporous and Mesoporous Mater.* **2012**, 156, 217–223.